JOURNAL OF AIRCRAFT
Vol. 49, No. 5, September–October 2012

# Experimental Study of an Extremely Flexible Rotor for Microhelicopters

Jérôme Sicard* and Jayant Sirohi†
*University of Texas at Austin, Austin, Texas 78712*

DOI: 10.2514/1.C031643

**This paper describes the development and testing of a rotor with extremely flexible blades, focusing on application to a microhelicopter. The goal is to develop rotor blades that are so flexible that they can be rolled into a compact volume and stowed inside the rotor hub. The design of an 18-in-diameter two-bladed rotor with flexible blades is presented. Stiffening and stabilization of the rotor blades are enabled by centrifugal forces acting on a tip mass. The relationship between blade-design parameters, aeroelastic stability boundaries, and hover performance is explored by a systematic set of experiments. It is observed that rotational speed and collective pitch angles have a significant effect on rotor stability. In addition, a large negative spanwise twist is induced in the flexible blades during stable operation, resulting in a decreased efficiency compared with rigid rotor blades having an identical planform and airfoil section. Different approaches to passively tailor the induced twist distribution are investigated. The highest efficiency was measured on a configuration making use of the propeller moment acting on a tip mass located at an index angle to the blade chord. A maximum figure of merit of 0.51 was measured at a blade loading of 0.14, which is comparable to the efficiency of rigid rotor blades.**



## Introduction

THE beginning of the 21st century has seen the emergence of a new class of vehicles called micro aerial vehicles (MAVs). MAVs, as originally defined by the Defense Advanced Research Projects Agency [1], include any unmanned air vehicle whose length dimensions are less than 6 in. (15.2 cm) and whose gross takeoff weight is approximately 7 oz (200 g) or less. The development of MAVs was initiated to meet new military needs; potential missions include military intelligence, surveillance, and reconnaissance missions. A wide range of latent commercial applications also exist, which include police surveillance, damage assessment, and fire and rescue operations. Because of their size, MAVs are ideally suited to operate in indoor environments such as in buildings or caves.

Among the types of MAVs in development, rotary-wing MAVs play an important role. Similar to their full-scale counterparts, microhelicopters hover efficiently and possess precise landing capabilities, which suit them for surveillance missions in confined spaces [2,3]. However, there are several challenges inherent to their design that should be addressed before fully taking advantage of their benefits. These mainly relate to obstacle detection and avoidance, increasing mission endurance, and reduction in gust sensitivity during outdoor flight.

In complex, cluttered indoor environments, there is a high likelihood of blade collision with obstacles. In this event, a rotary-wing MAV with conventional rigid rotor blades would sustain permanent blade damage and may crash upon impact. Hover endurance is a key enabler for indoor surveillance missions and can be increased by increasing the rotor diameter. However, this decreases the ability of the MAV to access confined spaces. In addition, gust sensitivity is strongly dependent on the downwash velocity, which is a function of rotor diameter. The rotor diameter is typically determined to obtain the best performance when faced with these conflicting requirements.

Flexible, stowable rotor blades offer the possibility of increased mission adaptability. Upon collision, flexible blades increase the probability of vehicle survival and recovery because they can spring back to their natural position and are less likely to be permanently damaged. Flexible rotor blades can also provide the ability to modify the rotor diameter in-flight. Because of the negligible stiffness of its structure, the rotor blade can be rolled up into a cylindrical shape and be retracted into the rotor hub (Figs. 1a and 1b). As a result, the microhelicopter can morph its rotor over a range of diameters, resulting in a low hover power and the ability to access confined spaces as required. Finally, decreasing rotor diameter increases the downwash velocity and, hence, increases tolerance to gusts.

There have been several research efforts in the past focused on flexible helicopter rotor blades. However, a systematic investigation of the feasibility of flexible rotor blades for microhelicopters has not been reported in the literature to date. This paper describes the design and testing of an extremely flexible rotor with a diameter of 18 in.

## State of the Art

The variable-diameter, stowable rotor concept emerged in the 1960s as a means to achieve two goals. The first goal was to achieve high-speed cruise flight in full-scale helicopters by decreasing the rotor-tip speed or stowing the rotor in forward flight. Telescoping rotor concepts were proposed to address this issue [4]. The major advantage of the variable-diameter rotor was that the rotational speed remained constant, whereas the major disadvantage was the additional mechanical complexity and weight added to the rotor system. Other studies, including Roeseler [5] and Katzenberger and Carter [6], have described the analysis and hover testing of variable-diameter or even stowable flexible rotors made out of a mylar sheet or a thin metal ribbon. Although promising, these concepts were not pursued beyond the model stage in favor of other, lower-risk approaches to achieving high speeds.

A second goal was to develop structurally light helicopters capable of lifting heavy loads. Expandable flexible blades were attractive, as they propose a lightweight solution to decrease the disk loading by increasing the rotor diameter, and are also lighter than rigid rotor blades [7]. At NASA Langley Research Center, Winston [8,9] studied the behavior of a 30-ft-diameter rotor with extremely flexible blades constructed of a thin nonporous fabric airfoil surface attached to two steel rods to form the leading and trailing edges (Fig. 2). Pruyn

Received 26 August 2011; revision received 13 January 2012; accepted for publication 13 January 2012. 

*Graduate Research Assistant, Department of Aerospace Engineering and Engineering Mechanics; jerome.sicard@utexas.edu. Student Member AIAA.
†Assistant Professor, Department of Aerospace Engineering and Engineering Mechanics; jayant.sirohi@mail.utexas.edu. Member AIAA.


a) Blades extended b) Blades retracted

**Fig. 1 Stowable flexible rotor concept.**

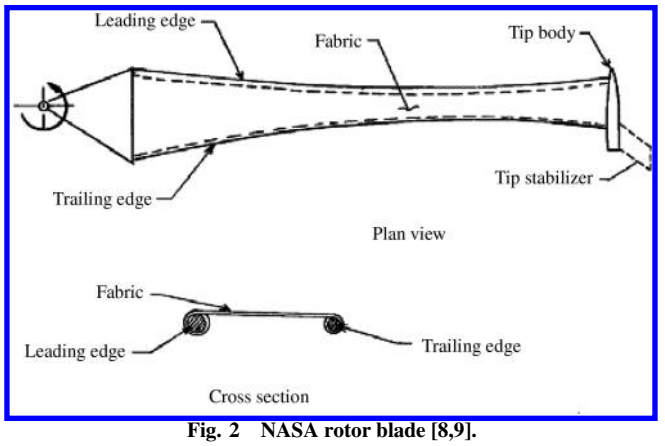


**Fig. 2 NASA rotor blade [8,9].**

and Swales [7] at Kellett Aircraft Corporation described the development and testing of a flexible rotor blade consisting of a fabric or stainless steel membrane between two cables that formed the leading and trailing edges (Fig. 3). At the Martin Company, Goldman [10] described the development and hover testing of an extremely flexible rotor. The rotor blades consisted of segmented balsa ribs with a flexible skin, supported by cables at the leading edge and trailing edge. The cables were attached to a tip pod with an electrically driven propeller that provided the torque required by the rotor.

The concept of flexible blades at the microhelicopter scale was investigated for the first time by Sirohi and Datta [11]. An 18-in.-diameter flexible rotor (Fig. 4) was constructed and tested in hover. The blades comprised a $\pm 90$ deg carbon-fiber ply impregnated with a flexible polyurethane elastomer. A tungsten rod 4.65 g in mass was secured to the blade tip. The hover performance of the flexible rotor was compared with that of a rotor with rigid blades having an

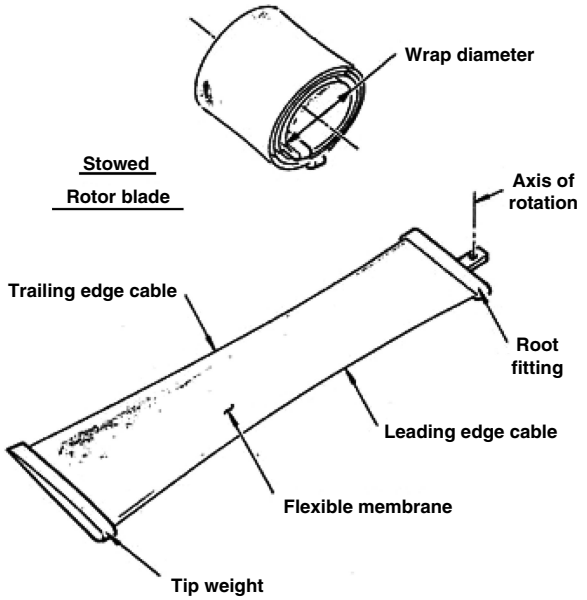


**Fig. 3 Kellett rotor blade [7].**

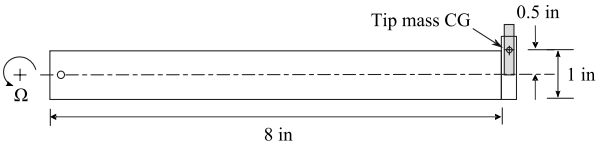


**Fig. 4 University of Texas at Austin flexible blade [11].**

identical planform and airfoil profile. Measurements indicated a maximum figure of merit (FM) of 0.44 for the rigid rotor blades and 0.22 for the flexible rotor blades. The low efficiency of the latter was attributed to a combination of an unfavorable twist distribution and large drag of the tip mass.

From these studies, it can be seen that the concept of an extremely flexible rotor that can be rolled up into a compact volume appears to be feasible. Efficiency of such rotor blades was found to be poor because of low chordwise stiffness of the blades, poor airfoil performance, and high drag of the tip mass. The limits of stability in hover and forward flight were not fully explored. Although the concept appears to be promising, limited data exist on their behavior, especially on the microhelicopter scale.

## Present Approach

The flexible-rotor concept proposed in this study (shown in the deployed state in Fig. 5) consists of a thin carbon-fiber composite sheet in conjunction with a tip body. The tip body increases centrifugal stiffening and stabilizes the rotor blade. The composite sheet is designed to sustain the centrifugal loads on the blade, eliminating the need for cables at the leading and trailing edges. The blade cross section is a circular arc, which is efficient at the low Reynolds numbers at which microhelicopters operate [2,3,12] ($Re \sim 5 \times 10^4$). Trailing-edge flaps provide primary control inputs to the rotor system and perform active stabilization. Finally, the tip body contains a miniature inertial measurement unit (IMU) with which the position and attitude of the blade tip can be measured at any instant of time. This IMU provides the sensory feedback for the stabilization and control of the flexible-rotor system.

This paper focuses on the behavior of the proposed flexible rotor in hover. The influence of various parameters on the stability and performance of flexible-rotor blades are investigated. The role of bending and torsional stiffness is explored by fabricating several sets of blades, using different combinations of composite fibers and resins. A detailed exploration of the dependence of control parameters such as collective pitch angle, speed of rotation, and mass balance on the stability of the blades is conducted. Additionally, attempts to reduce the drag of the tip mass are made. It is also expected that a twist will be induced along the blade span due to inertial moments [8,11]. Approaches to passively tailor the spanwise twist distribution are investigated. Although the proposed concept envisions the use of trailing-edge flaps and microactuators for active control, they are not explored in the present study. Rather, the goal is to optimize the efficiency of the rotor and explore its stability boundary.

## Physical Principles

The behavior of a rotor blade with extremely low structural stiffness is dominated by centrifugal forces. In particular, they stiffen the blade in the torsional degree of freedom in two ways: the dumbbell effect and the bifilar effect. The dumbbell effect (or tennis-racket effect) is also known as the propeller moment and arises due to

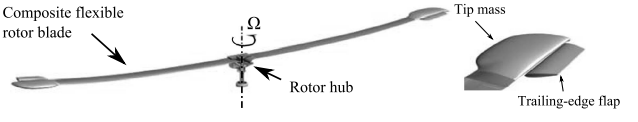


a) Flexible rotor in the deployed state b) Close-up view of the blade tip

**Fig. 5 Schematic of proposed flexible rotor blade.**

the tendency of the centrifugal forces to rotate the rotor blade to flat pitch. The bifilar moment, also known as the trapeze moment, arises from the twisting of the fibers, causing an effective shortening of the rotor blade. In conventional rotor blades, the propeller moment is dominant. However, in the present case, the bifilar moment can be significant due to the high torsional flexibility of the rotor blade. These two effects can be illustrated by a simple example.

We consider the case of a flexible rotor blade of constant chord, consisting of a tip mass supported by two cables, forming the leading and trailing edges of the blade. The plan view of such a blade is shown in Fig. 6. The tensile forces in each of the cables give rise to a torsional moment on the rotor blade equal to

$$M_\theta = F_1 \sin\phi_1 l \cos\theta + F_2 \sin\phi_2 (c-l)\cos\theta \tag{1}$$

$$\simeq \left(1-\frac{l}{c}\right) m_T \Omega^2 R \sin\phi_1 l + \frac{l}{c} m_T \Omega^2 R \sin\phi_2 (c-l) \tag{2}$$

where $l$ is the position of the center of gravity of the tip mass, $c$ is the blade chord, $m_T$ is the tip mass, $R$ is the blade radius, and $\Omega$ is the rotational speed. $\phi_1$ and $\phi_2$ are the angles between the tangent to the cables at the point of attachment to the tip mass and the horizontal plane. It can be deduced that the effective elastic axis of the blade is defined by the chordwise position of the center of gravity of the tip mass. In the general case, it can be shown that the elastic axis of the rotor blade is defined by the chordwise position of the centroid of the radial stress field along the blade span [5,10]. Assuming a linear torsional deflection mode shape, the torsional stiffness due to the bifilar effect is

$$K_\theta = l(c-l) m_T \Omega^2 \tag{3}$$

and the rotating natural frequency corresponding to the linear deflection mode is

$$\frac{\omega_\theta}{\Omega} = \sqrt{\frac{m_T c^2}{I_T}\left(\frac{l}{c}-\frac{l^2}{c^2}\right)} \tag{4}$$

where $I_T$ is the torsional moment of inertia of the tip mass about its center of gravity. For a cylindrical tip mass of uniform density ($I_T = m_T c^2/12$), the maximum rotating torsional frequency occurs when the tip mass is centered between the two cables ($l/c = 0.5$). In this condition, the torsional frequency becomes $\omega_\theta/\Omega = \sqrt{3} = 1.732/\text{rev}$, where rev indicates revolution.

We then consider a blade with constant chord, rotating at constant speed $\Omega$ (Fig. 7). The chordwise component of the centrifugal force creates the propeller moment, which is equal to

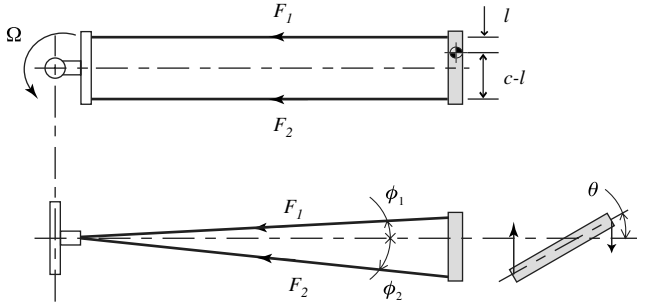


**Fig. 6 Schematic of bifilar moment in a flexible rotor composed of two cables.**

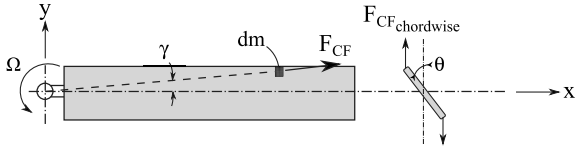


**Fig. 7 Schematic of propeller moment acting on a rotating blade.**

$$M_p = I_\theta \Omega^2 \theta \tag{5}$$

Hence, the torsional stiffness due to the propeller effect is

$$K_\theta = I_\theta \Omega^2 \tag{6}$$

and the corresponding rotating natural frequency is

$$\frac{\omega_\theta}{\Omega} = 1 \tag{7}$$

Although no detailed and specific aeroelastic analysis of a rotor with such low structural stiffness has been reported in the literature, simple studies, such as the one described by Winston [8], were performed considering a two-dimensional airfoil section undergoing vertical translational and pitching motion. As a result, the flutter and divergence boundaries for a rotor blade of low mass per unit length, of infinite flexibility in bending and torsion, and with cables as the main structural members were identified. Under these assumptions, Winston found that, to achieve stable operation for any value of tip mass, the elastic axis should be ahead of the aerodynamic center, and the blade section center of gravity should be ahead of the elastic axis. Although these assumptions are not valid for the blades considered in the present study, all the blades were designed so that their center of gravity was located ahead of the aerodynamic center (approximated to be at the quarter-chord point for thin cambered profiles [13]). This was achieved by adjusting carefully the chordwise location of the tip mass. The location of center of gravity also influences the twist induced along the span of the blade. In particular, a high twist due to propeller and bifilar moments is expected. Consequently, we are interested in two ways to passively tailor the twist distribution: 1) twist control by means of composite-material coupling and 2) tip twist imparted by use of propeller moment.

#### Twist Control by Means of Composite-Material Coupling

Preliminary qualitative observation of the prototype flexible rotor in hover indicated a large nose-down- induced twist. This leads to large portions of the blade being stalled. The objective is to develop a flexible rotor blade with an extension-torsion coupled composite laminate designed such that the unfavorable negative twist distribution is passively alleviated during hover. The centrifugal force acting on the tip mass in conjunction with an appropriate composite lay-up is expected to generate the desired twist deformations. The baseline blade [11] is an uncoupled laminate with no means to control the twist distribution. First, the collective pitch angle corresponding to the maximum FM of this baseline design, $\theta_{\text{eff}}$, is identified. When spinning in this condition, the tip of the baseline blade rotates at flat pitch. To minimize the unfavorable twist, the goal of the composite coupling is to produce a nose-up moment that results in a twist angle at the tip of $\theta_{\text{eff}}$ deg.

Figure 8 is a free-body diagram showing forces and moments applied on the tip of the flexible blade in rotation. The equations of equilibrium are as follows:

$$N_x = F_{\text{CF}} \tag{8}$$

$$M_{ss} = -M_p \tag{9}$$

At any spanwise location, the total centrifugal force and total propeller moment (nose down) are given by

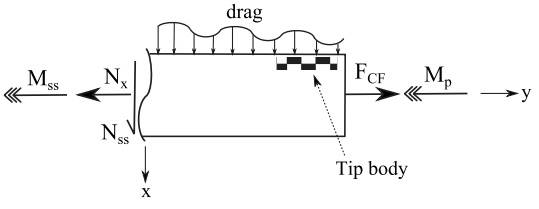


**Fig. 8 Free-body diagram of the rotating blade.**

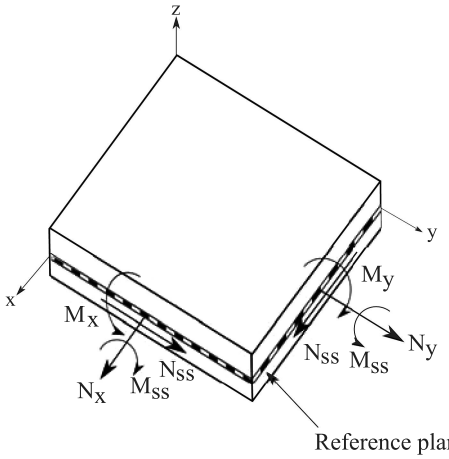


**Fig. 9 Laminated element with force and moment resultants.**

$$F_{\mathrm{CF}} = \int_y^R \Omega^2 m_y y \,\mathrm{d}y + m_T \Omega^2 R \tag{10}$$

$$M_p(y) = I_\theta \Omega^2 \theta (R - y) + I_T \Omega^2 \theta_T \tag{11}$$

where $y$ is the spanwise coordinate, $m_y$ is the mass per unit length, and $\theta_T$ is the angle of twist at the blade tip. Inertial forces on the blades are ignored with respect to the inertial forces on the tip mass. Thus, the propeller moment and centrifugal force acting on the blade airfoil are neglected compared with the propeller moment and centrifugal force acting on the tip mass.

For a general composite laminate, the forces and moments shown in Fig. 9 are related to reference plane strains and curvatures [14] as follows:

$$\begin{Bmatrix} N_x \\ N_y \\ N_{ss} \\ M_x \\ M_y \\ M_{ss} \end{Bmatrix} = \begin{bmatrix} [A] & [B] \\ [B] & [D] \end{bmatrix} \begin{Bmatrix} \epsilon_x^o \\ \epsilon_y^o \\ \gamma_s^o \\ \kappa_x \\ \kappa_y \\ \kappa_{ss} \end{Bmatrix} \tag{12}$$

where $[A]$, $[B]$ and $[D]$ are, respectively, the extensional, extensional-bending, and flexural-stiffness matrices. The $B_{xs}$ term in Eq. (12) is responsible for the extension–torsion coupling in the $x$ direction. As a matter of fact, for a nonzero $B_{xs}$, a normal force $N_x$ will cause the laminate to twist about the $x$ axis. To maximize the twist resulting from the coupling, the term $B_{xs}$ has to be maximized. The matrices $[A]$ and $[B]$ are a function of material properties, thickness, and orientation of the plies and are defined as

$$A_{ij} = \sum_{k=1}^{N} [Q_{ij}^{x,y}]_k t_k \tag{13}$$

$$B_{ij} = \sum_{k=1}^{N} [Q_{ij}^{x,y}]_k t_k \overline{z_k} \tag{14}$$

where the subscript $k$ is summed over the total number of plies, and $[Q^{x,y}]_k$ is the stiffness matrix of the $k$th layer, expressed in the $(x, y)$ system of coordinates (see Fig. 10).

As presented by Winckler [15], we consider a $[+\theta/-\theta]$ antisymmetric angle-ply laminate, which is known to exhibit strong extension–torsion coupling. If the two layers are considered separately, they are each symmetric with no extension–torsion coupling. However, for both plies, the term $A_{xs}$ is nonzero and is responsible for the extension–shear coupling. The extension–torsion coupling is generated when the two antisymmetric plies are bonded.

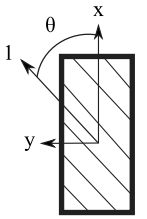


**Fig. 10 Coordinate systems of a generally orthotropic material.**

For a given normal tensile force, the largest twist will be obtained when $A_{xs}$ is at a maximum. Using Eq. (13), we obtain

$$\begin{aligned} A_{xs} = tQ_{xs} = t[&Q_{11}\cos^3\theta \sin\theta - Q_{22}\cos\theta \sin^3\theta \\ &+ Q_{12}(\cos\theta \sin^3\theta - \cos^3\theta \sin\theta) \\ &+ 2Q_{66}(\cos\theta \sin^3\theta - \cos^3\theta \sin\theta)] \end{aligned} \tag{15}$$

where $Q_{11}$, $Q_{22}$, $Q_{12}$, and $Q_{66}$ are related to the material properties of the lamina.

From Eq. (15), the coupling coefficient $A_{xs}$ can be plotted as a function of the fiber orientation $\theta$. It is observed that the largest twist deformations due to extension–torsion coupling will be obtained for the antisymmetric angle-ply laminate: $[+33/-33$ deg$]$. It can be noted that increasing the number of layers (i.e., $[+33/-33$ deg$]_n$) is unfavorable as the coupling stiffness $B_{xs}$ decreases in inverse proportion to the number of plies for the same overall thickness of the laminate.

To decide whether the extension–torsion coupling can balance the unfavorable twist due to the propeller moment acting on the tip mass, the load-deformation Eq. (12) must be inverted. The result is

$$\begin{Bmatrix} \overset{\epsilon}{\sim}{}^o \\ \overset{\kappa}{\sim} \end{Bmatrix} = \begin{bmatrix} [a] & [b] \\ [c] & [d] \end{bmatrix} \begin{Bmatrix} \overset{N}{\sim} \\ \overset{M}{\sim} \end{Bmatrix} \tag{16}$$

where the matrices $[a]$, $[b]$, $[c]$, and $[d]$ are the laminate compliance matrices. Then, the twist curvature can be expressed as

$$\kappa_{ss} = c_{sx}N_x + c_{sy}N_y + c_{ss}N_{ss} + d_{sx}M_x + d_{sy}M_y + d_{ss}M_{ss} \tag{17}$$

Only the terms associated with the propeller moment and the centrifugal force are retained in Eq. (17). This is justified by the fact that the magnitudes of pitching moments produced by aerodynamic forces are small compared with the one produced by the inertial forces. Using Eqs. (8) and (9), the twist curvature at the tip of the blade is

$$\kappa_T = c_{sx}(m_T \Omega^2 R) - d_{ss}(I_T \Omega^2 \theta_T) \tag{18}$$

Using numerical values for the present blade (summarized in Table 1), the overall twist curvature at the blade tip is found to be

$$\kappa_T = -0.21[\mathrm{m}^{-1}] \tag{19}$$

The corresponding angle of twist at the blade tip (assuming a linear twist along the spanwise direction) is

$$\theta_{\mathrm{Tip}} = -2.7 \text{ deg} \tag{20}$$

Without consideration of extension–torsion coupling, $\theta_{\mathrm{Tip}} = -2.8$ deg. As a result, it can be seen that the magnitude of the centrifugal force

**Table 1 Parameters of the baseline blade [11]**

| $\Omega$, rad/s | $\theta_T(=\theta_{\mathrm{eff}})$,deg | $m_T$, g | $R$, cm | $I_T$, gm.cm$^2$ | $c_{sx}$, (N.m)$^{-1}$ | $d_{ss}$, (N.m$^2$)$^{-1}$ |
|---|---|---|---|---|---|---|
| 157 | 21.0 | 4.65 | 22.6 | 3.83 | $2.624 \times 10^{-3}$ | $6.276 \times 10^{1}$ |

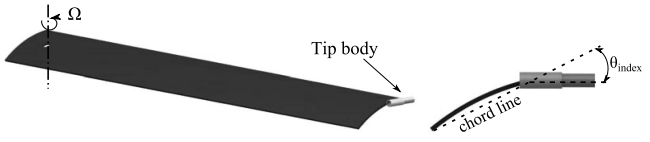


a) Flexible blade BP b) Cross section

**Fig. 11 Concept B: flexible rotor blade BP.**

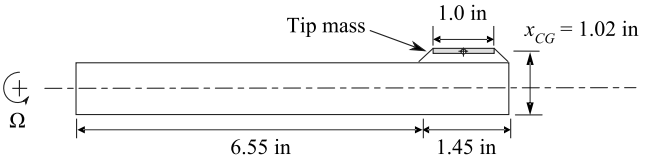


**Fig. 12 Planform of flexible blade C.**

produced by the tip mass is too small to produce a twist curvature capable of balancing the negative induced twist. It is not desirable to increase the mass of the tip body as it would decrease the weight efficiency of the rotor. It is concluded from this approach that extension–torsion coupling cannot be used as a way to tailor the twist distribution. Other forms of composite coupling can be investigated. In particular, bending–torsion coupling can be explored to stabilize the rotor. However, this requires a refined analysis to identify the lift distribution across the blade span.

#### Tip Twist Imparted by Use of Propeller Moment

The goal of this concept is to make use of the propeller moment acting on the tip mass to produce an untwisted rotor blade during hover operations. The baseline design [11] is modified by securing the tip mass oriented perpendicular to the blade span at an angle equal to $\theta_{\text{index}}$ deg with respect to the blade chord (Figs. 11a and 11b). The angle $\theta_{\text{index}}$ is the collective pitch corresponding to the maximum efficiency in hover of the baseline blade. It is expected that, while in rotation, the propeller moment acting on the tip body will align its longitudinal axis with the plane of rotation, making the flexible blade untwisted. For future reference, this design is labeled "Flexible blade BP".

## Blade Design and Fabrication

Multiple sets of flexible blades having similar planform and untwisted airfoil of constant chord were fabricated in-house.

A first objective was to decrease the profile drag created by the tip mass. Accordingly, a set of flexible rotor blades, featuring an alternate orientation of the tip body, was designed. The axis of the tip mass was set parallel to the span of the blade (Fig. 12). These composite blades were fabricated out of carbon fiber using a wet lay-up process. One ply of aramid fibers held the tip body and was enclosed between the two plies of carbon-fiber cloth. The laminae were compressed in a mold made out of acrylonitrile butadiene styrene. Blades with different bending and torsional stiffnesses were fabricated to explore their effect on stability and performance. This was achieved by varying the matrix and fiber orientation. The different types of blades are summarized as follows: 1) blade C1: flexible epoxy resin (Aircraft Spruce AlphaPoxy), 0/90 deg (2 plies) uncoupled carbon fiber; 2) blade C2: polyurethane elastomer (Freeman 1035), 0/90 deg (2 plies) uncoupled carbon fiber; and 3) blade C4: flexible epoxy resin (Aircraft Spruce AlphaPoxy), ±45 deg (2 plies) uncoupled carbon fiber.

As a result, the blades C1 were torsionally soft but stiff in bending, whereas the blades C2 were extremely soft, both in torsion and in bending (see Figs. 13a and 13b). The blade C4 had identical bending and torsional stiffnesses as blades C1 but could be rolled up with a smaller radius of curvature.

The mechanical properties of the laminates that resulted from impregnating two plies of uniaxial carbon fiber with the mentioned already matrices were determined through a set of tensile tests and are given in Table 2. Note that the elastic moduli of the composite with the Alphapoxy matrix are higher than that of the elastomer matrix. Hence, blades of different stiffnesses could be fabricated by varying the matrix. Because of the extreme flexibility of these blades, none of their nonrotating frequencies could be measured.

Blade BP is an iteration of the baseline blade [11] and is designed to address the problem of twist deformation. A schematic was shown in Figs. 11a and 11b. To secure the tip mass, a 0.002-in.-thick rectangular brass plate was inserted at the leading edge of the midply of the carbon/Alphapoxy laminate. The tip mass was then soldered to the brass shim. The resulting blade is shown mounted on the hover test stand in Fig. 14.

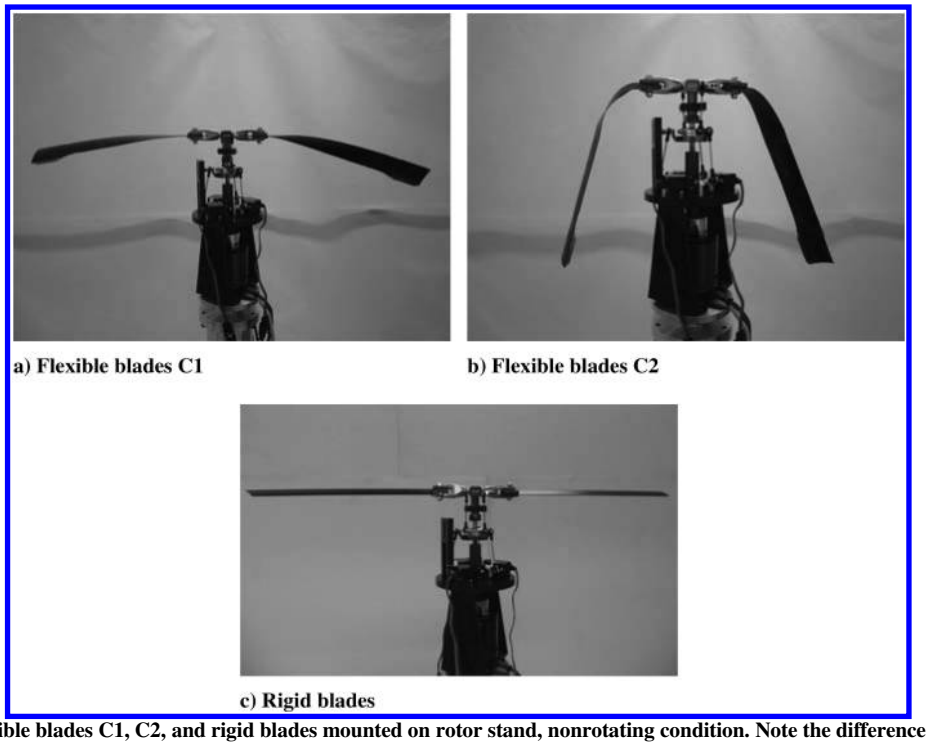


**Fig. 13 Flexible blades C1, C2, and rigid blades mounted on rotor stand, nonrotating condition. Note the difference in flexibility.**

**Table 2 Mechanical properties of the composite materials used in flexible-blade fabrication**

| | Carbon fiber/ elastomer | Carbon fiber/ Alphapoxy© |
|---|---|---|
| Tensile modulus $E_1$, GPa | 20.3 | 25.0 |
| Tensile modulus $E_2$, GPa | 0.1 | 0.1 |
| Shear modulus $G_{12}$, GPa | 0.46 | 1.54 |
| Poisson ratio | 0.3 | 0.3 |
| Mass per unit area, g/cm$^2$ | 0.043 | 0.037 |

Rigid blades were fabricated using two plies of carbon-fiber cloth, oriented ±45 deg to the blade span. The plies were impregnated with a conventional room-temperature cure resin and were compressed in a mold. The resulting blades were stiff in torsion as well as in bending (Fig. 13c) and had the circular arc sectional profile imparted by the mold.

Table 3 summarizes the characteristics of each blade design. Note that rigid blades have higher thickness-over-chord ratio to ensure sufficient stiffness.

## Experimental Setup and Test Procedure

The performance of the blades in hover was measured on a test stand designed and built in-house. The two-bladed rotor hub was mounted directly on a brushless outrunner direct current motor. The motor (Hacker A50 16S) was chosen to have a high torque and low-speed constant so that it could directly drive a rotor of diameter up to 0.6 m at a tip speed of up to 135 m/s without the need for a gearbox. A swashplate assembly operated by three high-speed digital servos allowed for precise adjustment of the rotor collective and cyclic pitch angles. The motor and rotor assembly was mounted directly on a six-component strain gage load cell (ATI Mini40E), with a full-scale rating of 5 lbs in the thrust direction. A magnetic pickup provided a 1/rev pulse, which was used to measure the rotational speed as well as to perform synchronous averaging of all the signals. This was also used to trigger a strobe light to illuminate the rotor and enable photography of the blades in-flight. In this way, stability boundaries as well as blade deformations could be observed visually. Data were acquired by a National Instruments CompactDAQ system with a custom virtual instrument programmed in Labview. The quantities measured were the rotor forces and moments in the fixed frame, rotational speed, motor voltage, and motor current.

The hover testing was performed at a constant rotor speed of 1500 rpm ($Re = 55,260$ at blade tip). The rigid and flexible blades were tested over a range of collective pitch angles from 0 to 30 deg.

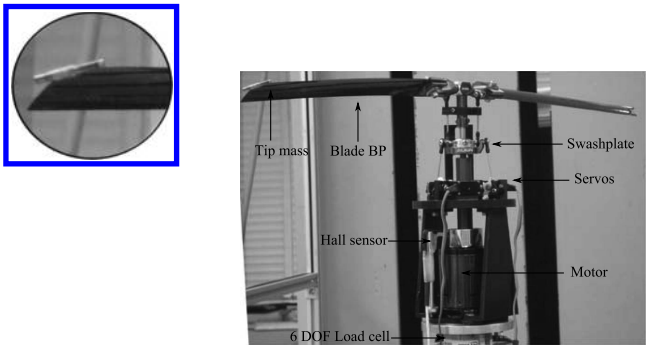


**Fig. 14 Flexible blades BP mounted on hover test stand.**

The goal of the hover tests was to measure the thrust generated by the flexible blades as a function of the collective pitch and to measure the efficiency of the rotors in terms of hover FM.

The region of stable operation of the blades was first identified. Previous studies [8,9] relied on changes in noise or vibration to determine the onset of instability. The present study used the strobe light to visually observe the blade deformation in-flight. In this way, any oscillations of an unstable blade could clearly be observed, although no blade motion was discernible for the stable blades. It was noted that, in several cases, there was no change in noise in spite of visual evidence of instability. No data were collected in the cases where the rotor was unstable.

## Results and Discussion

### Aeroelastic Stability

The flexible rotor concepts presented in this paper were designed such that the center of gravity at each blade section was located forward of the quarter-chord point. Previous analytical studies have indicated that this condition was sufficient to ensure a blade free from pitch-flap flutter and pitch divergence, regardless of the rotor speed [8–10]. However, experimental data show that this stability criterion is invalid for the types of blades presented in this study. The sharp transition between a stable regime and unstable operations of the rotor is shown in Fig. 15. The photographs were taken using a long exposure, resulting in the blade position being recorded over multiple rotor revolutions. The blurred image indicates that the corresponding regions of the blade are undergoing motion at a frequency noninteger multiple of 1/rev.

It appeared that pitch-flap flutter instability of the flexible rotors was not only dictated by the rotational speed of the rotor, but also by the collective pitch angle. Figure 16 shows the pitch-flutter stability

**Table 3 Blade design matrix**

| Design | Schematic planform | Material | Rotor radius, in. | Chord, in. | Thickness, in. | Camber, % | $t/c$ ratio, % | Airfoil mass, g | Tip body mass, g | Total blade mass, g |
|---|---|---|---|---|---|---|---|---|---|---|
| B | 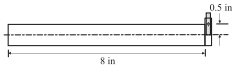 | Carbon fiber/ elastomer | 9 | 1 | 0.03 | 7.5 | 3 | 5.85 | 4.40 | 10.25 |
| C1 | | Carbon fiber/ Alphapoxy | 9 | 0.9 | 0.015 | 7.5 | 1.7 | 2.20 | 2.15 | 4.35 |
| C2 | 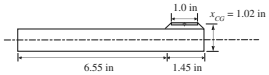 | Carbon fiber/ elastomer | 9 | 0.9 | 0.020 | 7.5 | 2.2 | 3.10 | 2.15 | 5.25 |
| C4 | | Carbon fiber/ Alphapoxy (±45 deg wrt. span) | 9 | 0.9 | 0.015 | 7.5 | 1.7 | 2.35 | 2.15 | 4.50 |
| BP | 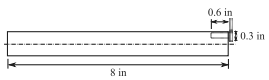 | Carbon fiber/ Alphapoxy | 9 | 0.95 | 0.010 | 7.5 | 1.1 | 2.00 | 2.30 | 4.30 |
| Rigid blade | 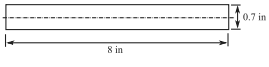 | Carbon fiber/ resin epoxy | 9 | 0.7 | 0.025 | 5.5 | 3.6 | 4.65 | $N/A$ | 4.65 |

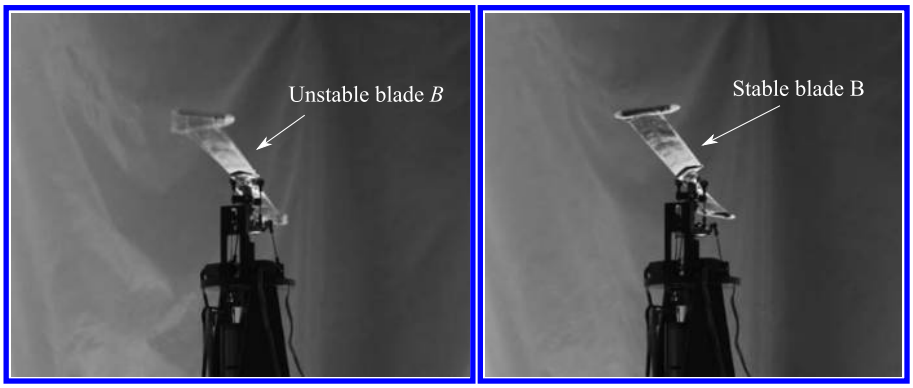


**a) Unstable blade B, 1500 RPM, $\theta_\circ = 0°$.** **b) Stable blade B, 1500 RPM, $\theta_\circ = 10°$**

**Fig. 15 Pitch-flutter and stable operations of the blades B.**



boundary of blade C1. For a collective pitch angle greater than 7.5 deg, the rotor is always stable. It should be observed that previous analyses of the aeroelastic stability of flexible blades assumed infinitely small torsional and bending stiffnesses. This hypothesis implies that the blade cannot sustain its own weight in the nonrotating condition, which is invalid for the design C1 (see Fig. 13a). The blades C2 fabricated using flexible elastomer approximate an infinitely flexible rotor. Experimentally, it was observed that the blade was unstable for collective pitch angle in the range 0 to 25 deg and then stable for very high collective pitch angles above 30 deg.

Another key observation is that the incident velocity does not adversely affect the stability of a flexible rotor tested in forward flight. On the contrary, it is found to increase the region of stability. As the blades C1 were tested at advance ratios between 0.05 and 0.25, it could be seen that unstable rotors in hover condition were stable in forward flight.

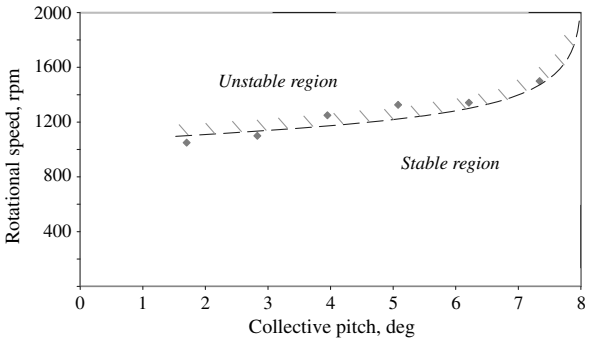


**Fig. 16 Stability boundary of rotational speeds and collective angles: blade C1.**

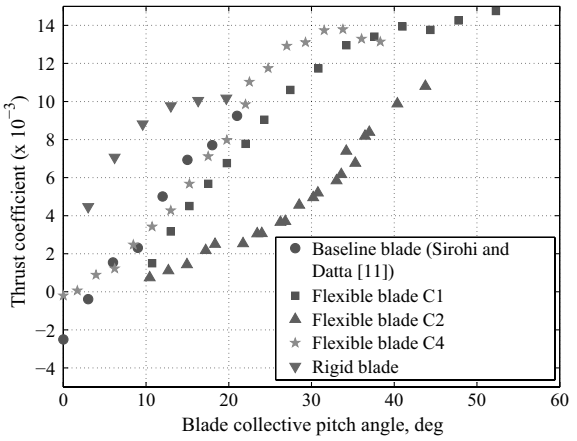


**Fig. 17 Comparison of thrust coefficients of rigid and flexible rotors at 1500 rpm.**

From these observations, it can be assumed that the source for the instability may be associated with the returning wake of the rotor. One of the possible instabilities is called wake-excited flutter and is known to occur under the operating conditions for which the returning wake has the strongest influence: low collective pitch, low forward speed, or hover [16].

To accurately model the stability and behavior of a flexible microhelicopter rotor blade, a refined comprehensive aeromechanics code focused on large displacements, and very low material stiffness has to be developed from first principles.

### Rotor Performance in Hover

Figure 17 shows the thrust coefficient in hover as a function of collective pitch angle. Stall is indicated by the change in the slope of the thrust-coefficient curve. It can be noted that the stiffer the blade is in torsion, the lower the collective pitch is at which stall occurs. This is because of high twist angles induced in the flexible blades, as seen in Fig. 18. The outboard section of the blades that is responsible for the greatest percentage of thrust remains unstalled. In the case of the flexible blades, forces and moments were not measured for collective pitch angles below 10 deg because the rotors were not stable at these angles at 1500 rpm. However, the slope of the thrust-coefficient curves indicates that, if the blades had been stable, they would have generated a negative thrust. This result is attributed to the nose-down torsional moment caused by the weight of the tip mass, resulting in a net negative twist of the rotor blade and a negative angle of attack at the outboard locations.

From Fig. 17, it can be seen that flexible rotors are capable of generating as much thrust or more than rigid rotors. The maximum thrust coefficient is obtained for the blades C1 and C4 and is equal to 0.014.

Figure 19 shows the FM of each rotor as a function of blade loading. As expected, the rigid rotor blades are the most efficient, and their maximum FM is approximately 0.50 for a blade loading of 0.15.

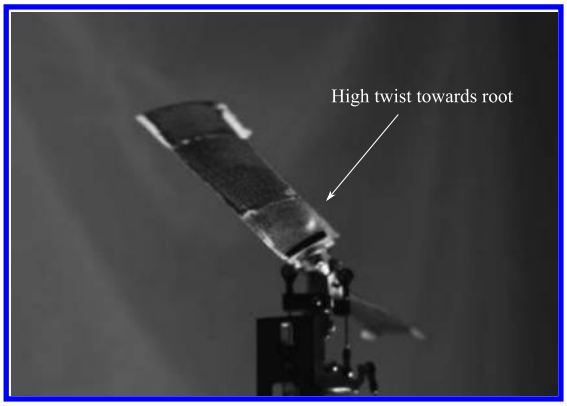


**Fig. 18 High induced twist angle at the inboard section of blade C2 at 1500 rpm, $\theta_0 = 16$ deg.**

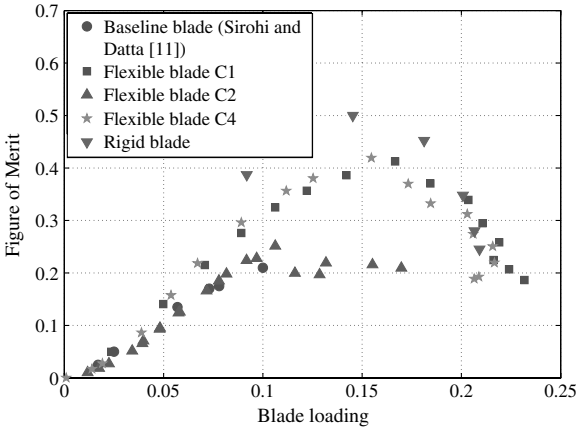


**Fig. 19 Comparison of FM of rigid and flexible rotors at 1500 rpm.**

The best FM for a flexible blade is achieved by the design C4 (carbon-fiber/AlphaPoxy, oriented ±45 deg with respect to the span) and is equal to 0.41. This value is twice the maximum FM obtained for the baseline blade. This enhancement comes mainly from the change in material rather than the change in tip-mass location and the associated drag. Indeed, the maximum FM of the blade C2 (carbon-fiber/elastomer) is only 0.25, representing an increase of only 0.05 compared with the baseline blade, which is made out of the same composite material.

To improve the efficiency, it is necessary to control the twist distribution. The potential benefit on the performance of the design BP is now evaluated. Figure 20 shows the FM of the flexible blade BP. It is compared with the FM of the identical flexible rotor blade whose tip mass is aligned with the chord of the airfoil [11] as well as a conventional rigid rotor having the same planform. It can be seen that the index angle between the tip mass and the chord has a favorable effect on the rotor efficiency. The maximum FM of the present design is equal to 0.51 for a blade loading of 0.14, which is more than twice that of the baseline blade. This improvement is related to the control of the twist along the blade span, which almost vanishes at optimum operation of blade BP (see Fig. 21). The maximum FM is obtained at a collective pitch angle of 16 deg. Thus, a new iteration where the index angle is equal to 16 deg has to be made to totally eliminate the twist due to propeller moment.

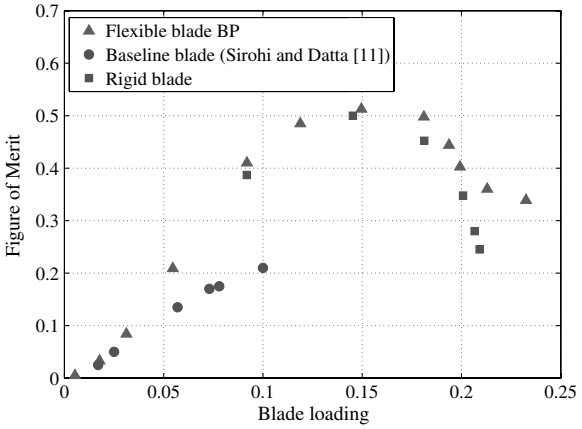


**Fig. 20 FM of the flexible blade BP.**

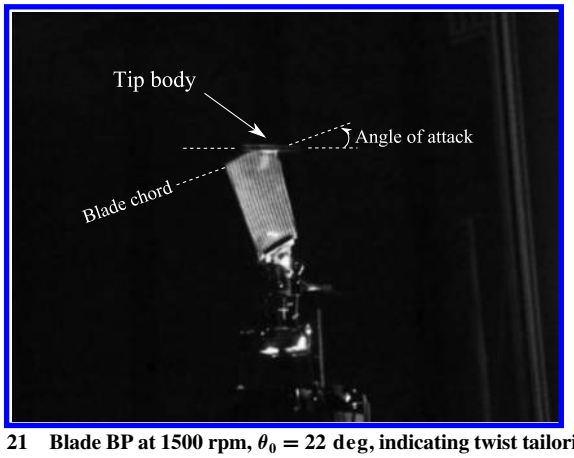


**Fig. 21 Blade BP at 1500 rpm, $\theta_0 = 22$ deg, indicating twist tailoring.**

Finally, these results demonstrated that microhelicopter blades fabricated with a flexible resin such as the AlphaPoxy offer a good compromise between rigid rotor blades and extremely flexible blades made out of elastomer. The performance of such a rotor is close to that of a rigid rotor, and it has sufficient flexibility to be impact-resistant as well as amenable for a varying rotor-diameter design.

## Conclusions

The goal of this study was to develop rotors with blades so flexible that they could be rolled up and stowed inside the rotor hub. The design of the rotor blades was focused toward application on a microhelicopter. Accordingly, the blades have a circular arc airfoil section with 7.5% camber; untwisted, constant chord planform; and a span consistent with a rotor diameter of 18 in. A tip mass is used to stabilize the flexible rotor.

A systematic experimental investigation was conducted to define the planform, mass distribution, and materials of an efficient flexible rotor. Rotor blades of different stiffnesses were fabricated and tested. Two designs appeared to be the most efficient. The first one incorporates a tip body comprising a 1-in.-long tungsten rod aligned with the spanwise direction of the blade and located at the leading edge. The mass of the airfoil is of the same order as the tip mass, and the overall mass of the blade is 4.35 g. The tip body is placed so that the overall center of gravity of the blade is ahead of the quarter-chord point. Although previous analytical studies related to extremely flexible rotors had concluded that rotor stability was independent of the rotational speed, it was found experimentally that the collective pitch angle, rotational speed, and incident velocity have a significant effect on stability. Stall of the flexible rotor was observed to occur at a very high collective pitch angle of 40 deg. At that point, the inboard section of the blade was highly twisted. A maximum figure of merit of 0.41 was measured. In comparison, a rigid rotor of the same diameter and solidity has a maximum figure of merit of 0.5. The poor efficiency of the flexible blades is attributed to an unfavorable twist distribution along the blade span, which is caused by the combination of the propeller moment and the gravitational force acting on the tip body.

Accordingly, the design was modified to passively tailor the spanwise twist distribution. The objective was to make use of the propeller moment acting on the tip mass to produce an untwisted rotor blade during hover operation. A tungsten rod oriented perpendicularly to the blade span was secured at the blade tip, and its longitudinal axis made an angle of 22 deg with respect to the blade chord. The performance was significantly improved. A maximum figure of merit of 0.51 was computed at a blade loading of 0.14.

Finally, as a second approach to balance the nose-down propeller moment, extension–torsion composite coupling was investigated. The goal was to make use of the centrifugal force produced by the tip mass to generate nose-up twist deformations. It was found that a $[+33/-33$ deg] composite laminate generates the largest twist curvature for a given normal force. However, the magnitude of the centrifugal force is too small to balance the negative twist curvature due to the large propeller moment.

Future plans involve the development of a comprehensive aeromechanics analysis capable of modeling large deformations and blades with very low stiffness. The analysis will be validated with the experimental results obtained in the present study. In addition, the design of a trailing-edge flap will be investigated as a means to control twist deformations at the blade tip. Finally, other forms of composite-material coupling, such as bending–torsion coupling, will

be investigated to extend the stability boundaries of extremely flexible rotor blades.

## References


[1] Davis, W. R., Jr., Kosicki, B. B., Boroson, D. M., and Kostishack, D. F., "Micro Air Vehicles for Optical Surveillance," *Lincoln Laboratory Journal*, Vol. 9, No. 2, 1996, pp. 197–214.

[2] Pines, D. J., and Bohorquez, F., "Challenges Facing Future Micro Air Vehicle Development," *Journal of Aircraft*, Vol. 43, No. 2, Apr. 2006, pp. 290–305. doi:10.2514/1.4922

[3] Chopra, I., "Hovering Micro Air Vehicles: Challenges and Opportunities," *Proceedings of American Helicopter Society Specialists' Conference/International Forum on Rotorcraft Multidisciplinary Technology*, American Helicopter Society, Seoul, Korea, 15–17 Oct. 2007.

[4] Fradenburgh, E. A., "The High Speed Challenge for Rotary Wing Aircraft," *29th International Pacific Air & Space Technology Conference*, SAE Paper 911974, Nagoya City, Japan, Oct. 1991.

[5] Roeseler, W. G., "The Effect of Ribbon Rotor Geometry on Blade Response and Stability," Master's Thesis, Massachusetts Inst. of Technology, Cambridge, MA, May 1966.

[6] Katzenberger, E. F., and Carter, E. S., "Vertical Flight: The Age of the Helicopter," Smithsonian Instit. Press, Washington, D.C., 1984, pp. 193–219.

[7] Pruyn, R. R., and Swales, T. G., "Development of Rotor Blades with Extreme Chordwise and Spanwise Flexibility," *Proceedings of the American Helicopter Society 20th Annual National Forum*, American Helicopter Society, Washington, D. C., 13–15 May 1964, pp. 102–108.

[8] Winston, M. M., "An Investigation of Extremely Flexible Lifting Rotors," NASA TN D-4465, Apr. 1968.

[9] Winston, M. M., "A Hovering Investigation of An Extremely Flexible Lifting Rotor," NASA TN D-4820, Oct. 1968.

[10] Goldman, R. L., "Some Observations on the Dynamic Behavior of Extremely Flexible Rotor Blades," *28th Annual Meeting of the Industry Applications Society*, IAS Paper 60-44, New York, 25–27 Jan. 1960.

[11] Sirohi, J., and Datta, A., "Investigation of an Extremely Flexible Stowable Rotor," *Proceedings of the American Helicopter Society 65th Annual Forum*, American Helicopter Society, Grapevine, TX, 27–29 May 2009.

[12] Hein, B. R., and Chopra, I., "Hover Performance of a Micro Air Vehicle: Rotors at Low Reynolds Number," *Journal of the American Helicopter Society*, Vol. 52, July 2007, pp. 254–262.

[13] Abbott, I. H., and von Doenhoff, A. E., *Theory of Wing Sections*, 1st ed., McGraw–Hill, New York, 1949, pp. 69.

[14] Daniel, I. M., and Ishai, O., "Elastic Behavior of Multidirectional Laminates," *Engineering Mechanics of Composite Materials*, Oxford Univ. Press, Oxford, England, U.K./New York, 2006, pp. 164.

[15] Winckler, S. J., "Hygrothermally Curvature Stable Laminates with Tension-Torsion Coupling," *American Helicopter Society International Conference on Rotorcraft Basic Research*, American Helicopter Society, Research Triangle Park, NC, Feb. 1985, pp. 56–58.

[16] Anderson, W. D., and Watts, G. A., "Rotor Blade Wake Flutter – A Comparison of Theory and Experiment," *Journal of the American Helicopter Society*, Vol. 21, Apr. 1976, pp. 32–43. doi:10.4050/JAHS.21.32